# A HIERARCHICAL CONTROL SCHEME TO IMPROVE THE STABILITY AND ENERGY QUALITY OF A HYBRID WIND / PHOTOVOLTAIC SYSTEM CONNECTED TO THE ELECTRICITY GRID

Belkacem BELABBAS[1], Mouloud DENAI[2], Tayeb ALLAOUI[3]

*This paper presents an effective control scheme for a grid-integrated hybrid renewable energy system (HRES) consisting of wind and photovoltaic energy sources. The first layer of the general scheme includes five-level NPC converters in order to improve the quality of the energy produced by the HRES and use an advanced super twisting sliding mode controller to regulate the DC bus voltage. The second layer based on a hierarchical energy management structure for ensuring reliability and efficiency of the HRES. The simulation results showed good energy quality produced by the proposed HRES and efficient coordination between the HRES and the power grid.*

**Keywords**: Hybrid Renewable Energy System; Wind Energy; Photovoltaic Energy; Super Twisting Sliding Mode Controller; five-level NPC converters; Energy Management.

## 1. Introduction

The HRES have great potential to provide customers with better and more reliable energy supply than a single energy source system as combining two or more RES is likely to increase energy production [1], [2]. There are many ways of combining different RES to build a HRES either isolated or connected to the power grid. The main RES used are wind energy (WE) and solar photovoltaic energy (PVE).

The contribution of this article is to improve the reliability, stability and quality of energy produced by an HRES connected to the grid composed of a WE and PVE.

The HRES has proved to be a viable solution to help the electricity grid achieve an energy balance between generation and load demand [3]. HRES

[1] Department of Electrical Engineering, Laboratory of L2GEGI, University Ibn Khaldoun of Tiaret, Algeria, e-mail: belabbas.belkacem@univ-tiaret.dz

[2] Department of Electrical Engineering, School of Engineering and Computer Science, University of Hertfordshire, Hatfield, UK, e-mail: m.denai@herts.ac.uk

[3] Department of Electrical Engineering, Laboratory of L2GEGI, University Ibn Khaldoun of Tiaret, Algeria, e-mail: tayeb.allaoui@univ-tiaret.dz

connected to the grid are designed to cover their local electricity demand. Any surplus of energy can be either transferred to other consumers or exported to the power grid. Moreover, if the energy production from Renewable Energy Source (RES) cannot satisfy the local demand then the required power is imported from the grid [4].

The challenge of connecting a HRES to the power grid is largely solved by the use of power electronic converters which have the ability to manage the following features: Transfer the maximum power extracted by the HRES, protect the sources against sudden changes in load, control the powers injected into the grid and enhance the quality of energy produced. Due to the intermittency of RES, energy quality represents a potential challenge for HRES [5].

Multilevel converter topologies are extensively being used in high power applications and also in applications requiring improved power quality due to their ability to provide enhanced voltage waveforms with much lower harmonic levels. Different topologies of power converters have been proposed for power conditioning in RES. The Neutral-Point Clamped (NPC) topology has been the most commonly used topology in the development of high-voltage and high-power RES. It has many advantages such as better waveform of the output voltage, reduced Total Harmonic Distortion (THD) of the voltage and current which reduces the size of the output filter as compared to conventional two-level converters [6]. In this study, a five-level NPC converter is used.

The main drawback of these converters is the balancing the capacitor voltages of the DC link. To solve this problem, a control system has been proposed in the literature which consists of two loops [7]. The outer closed-loop controls the average value of the DC voltage using the conventional Proportional-Integral (PI) type controller, whereas the inner loop controls the difference between the two voltages in each half-arm using a clamping bridge circuit.

The conventional PI type controller is the most commonly used controller due to its simplicity of implementation. However, it cannot provide satisfactory performance under a wide range of operating conditions [8].

Nonlinear controllers based on Lyapunov stability have been successfully used in a variety of applications due to their robustness and performance. Among these is the Sliding Mode Controller (SMC) which has been widely employed due to its simplicity and ease of implementation. However, the main disadvantage of this control strategy is the presence of a chattering phenomenon [9], [10]. To eliminate chattering problem, several approaches have been described in the literature such as the Higher-Order Sliding Mode Controllers (HOSMC) [11], [12], the Fuzzy Sliding Mode Controller (FSMC) [13], [14] and the Super-Twisting Sliding Mode Controller (STSMC) [15]. In this work, the STSMC is used to control the DC link voltage of a five-level inverter.

To ensure a safe and reliable operation of the grid connected HRES, it is necessary to add a control and monitoring system to coordinate between the RES and the grid and maintain energy supply-demand balance.

The paper is organized as follows: Section 2 describes the general configuration of the proposed HRES. Section 3 presents the modeling and control of the DC bus of the five-level inverter. In Section 4, a HRES monitoring and supervision system is described. Finally, the results of the simulation and the conclusions are presented in Sections 5 and 6 respectively.

## 2. Configuration of the proposed RESH

Fig. 1 shows the general configuration of the HRES connected to the power grid. The WE and PVE conversion systems are rated 7.5 kW and 4.4 kW respectively. The powers generated by the HRES are either be consumed by the load or transferred to the power grid. In our study, the grid is considered an infinite backup system.

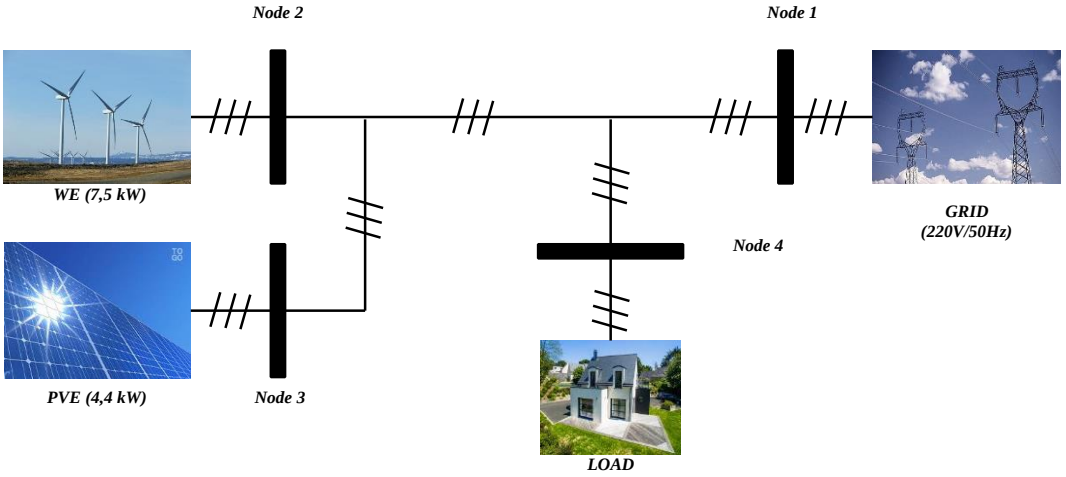


Fig. 1. The RESH connected to the grid.

### 2.1. Description of the WE

The Double-Fed Induction Generator (DFIG) with vector control has been widely used for large scale wind generation applications and is currently the dominant technology due to its advantages such as variable speed operation through the use of power converters, active and reactive power control for better integration into the power grid with reduced converter cost, simple design, inexpensive manufacturing, robustness, and low maintenance.

The Wind Energy Conversion System (WECS) used in this work is shown in Fig. 2. It consists of a wind turbine, a DFIG, two static converters cascaded through a DC bus in back-to-back configuration and a three-phase current filter.

To extract the maximum power from the WECS for different values of the wind speed, a Maximum Power Point Tracking (MPPT) strategy is used.

Different topologies of power converters have been proposed for power conditioning in WECS applications. Multilevel converters, especially the NPC topology, are being extensively used in the development of WECS.

The modeling and control of wind turbines based on DFIG are presented in detail in [16]–[17]. Also, the modeling and control of the five-level NPC inverter will be discussed in Section 5.

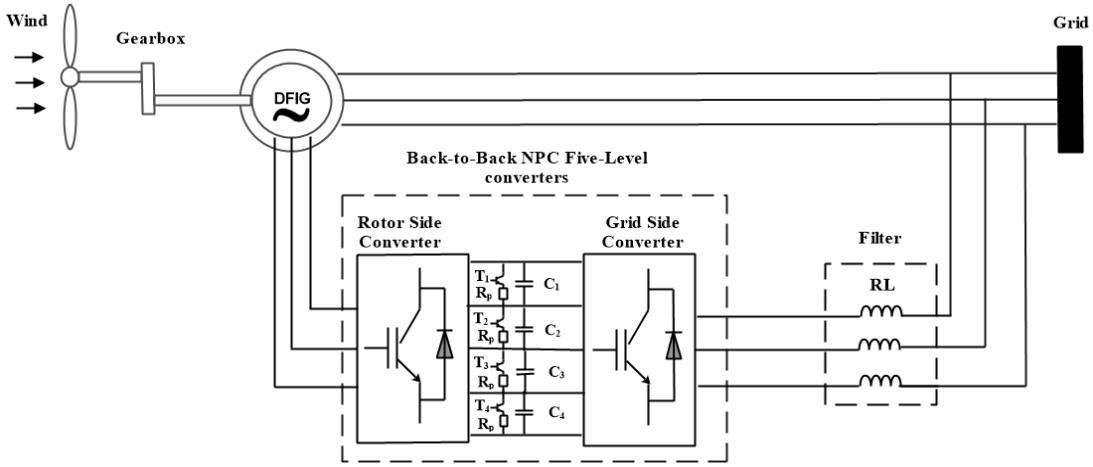


Fig. 2. Structure of the WECS based on the DFIG.

### 2.2. Description of the PVE

The PV Energy Conversion System (PVECS) connected to the electrical grid is shown in Fig. 3. It consists of the PV array, a DC-DC boost converter with MPPT control and a five-level NPC inverter. The five-level inverter is used to improve the quality of energy produced by the PVECS. Finally, a passive filter RL is connected between the output of the inverter and the electrical grid. The modeling of the PVECS and its control scheme are presented in detail in [18], [19], [20].

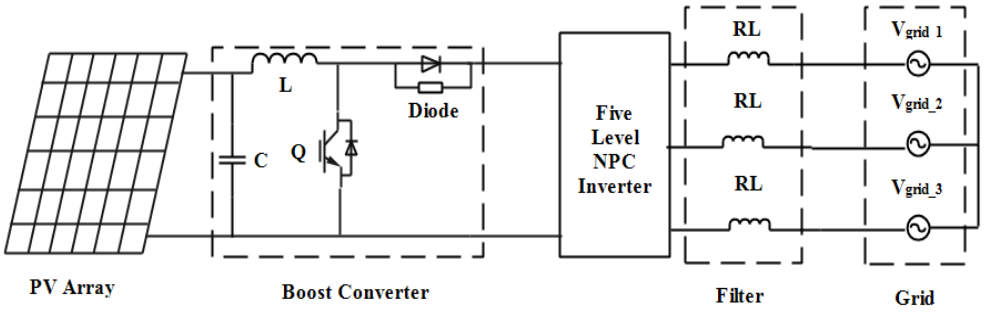


Fig. 3. Structure of the PVECS.

## 3. Presentation and control of Five-level NPC inverter

### 3.1. Presentation of Five-level NPC inverter

The five-level NPC inverter shown in Fig. 4 consists of four serial capacitors ($V_{C1}$, $V_{C2}$, $V_{C3}$, $V_{C4}$) forming a midpoint ($M$). This structure consists of three arms ($A$, $B$, $C$). Each of the three arms is composed of eight controlled switches ($T_{i1}$, $T_{i2}$, $T_{i3}$, $T_{i4}$, $T_{i5}$, $T_{i6}$, $T_{i7}$, $T_{i8}$) and two clamping diodes ($DD_{i1}$, $DD_{i2}$) for the arm. The modeling and PWM technique with four carriers for the five-level inverter are detailed in [21].

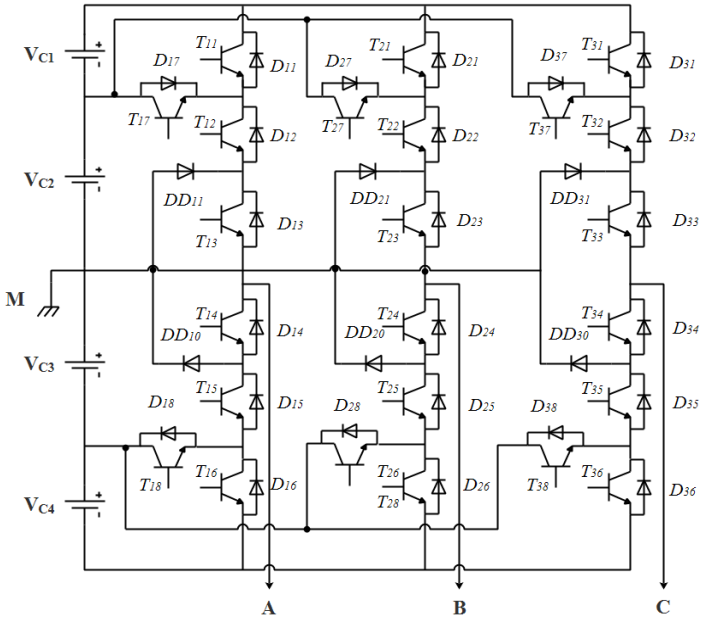


Fig. 4. Topology of the five-level NPC inverter.

### 3.2. Control strategy of the DC voltage for five-level NPC inverter

The unbalance of the input voltages of the five-level inverter causes the floating-point potential problem. In addition, to have a perfect operation of the inverter with five levels, these four input voltages must be constant and equal.

Two control strategies are employed to ensure the control and balance of DC voltages. The first strategy consists in controlling the average value of the DC voltage by an advanced non-linear regulator such as the STSMC type. The second strategy is based on a balancing bridge structure called clamping bridge for the purpose of controlling the difference between the two voltages in each half-arm.

#### 3.2.1. Nonlinear STSMC control design for DC voltage control

The principle of Sliding Mode Control (SMC) consists of attracting the dynamics of a system to the sliding surface and then switching using a control law to the point of equilibrium. The design of this controller considers stability issues and desired performance in a systematic way. The implementation of this control strategy is mainly carried out in three steps: (i) choice of the Surface, (ii) establishment of conditions of existence and convergence and (iii) determination of the control law. However, the main disadvantage of this command is the presence of chattering. To eliminate this problem, several approaches have been described in the literature. The STSMC has the ability to eliminate chattering while retaining the same tracking and robustness performance of the SMC.

In this section, the basic principle and design procedure of the DC link voltage controller based on STSMC are presented for a five-level inverter. The STSMC scheme consists of two terms: the equivalent control ($u_{eq}$) and super twisting control ($u_{st}$).

$$u(t) = u_{eq}(t) + u_{st}(t) \tag{1}$$

$$u_{st}(t) = u_1(t) + u_2(t) \tag{2}$$

$$\begin{cases} u_1(t) = -\lambda |S|^{1/2} \operatorname{sgn}(S) \\ u_2(t) = -\gamma \operatorname{sgn}(S) \end{cases} \tag{3}$$

Where: $\lambda$ and $\gamma$ are positive constants. $S$ defines the surface.

For the equivalent control of STSMC, the same procedure is used as for the conventional SMC. Its design procedure applied for a DC voltage control includes the following steps:

***A. Equivalent control***

The switching surface is designed as:

$$S(V_{DC}) = V_{DC}^{*} - V_{DC} \tag{4}$$

$$S(\dot{V}_{DC}) = \dot{V}_{DC}^{*} - \dot{V}_{DC} \tag{5}$$

In order to guarantee the existence of a sliding mode and to ensure convergence, the condition on the Lyapunov function must be fulfilled:

$$S(\dot{V}_{DC}).S(V_{DC}) \leq 0 \tag{6}$$

$$S(\dot{V}_{DC}) = \dot{V}_{DC}^{*} - \frac{1}{C} I_{DC} \tag{7}$$

The output of STSMC is the reference of the DC link voltage. So, the equivalent control is given by:

$$S(\dot{V}_{DC}) = 0 \Rightarrow I_{DC} = C.\dot{V}_{DC}^{*} \tag{8}$$

Where: $V_{DC}$ and $I_{DC}$ represent the voltage and current of the DC link. $V_{DC}$* is the reference of the DC link voltage

### *B. Super Twisting surface*

To eliminate the chattering phenomenon, a Super Twisting (ST) surface based on a "*tanh*" function is used. The ST surface is given by:

$$I_{DC(ST)} = -\lambda \left| S(V_{DC}) \right|^{1/2} \tanh(S(V_{DC})) - \int \gamma \tanh(S(V_{DC}) dt \tag{9}$$

The positive $\lambda$ and $\gamma$ are chosen to fulfil the condition of convergence.

The schematic diagram for the STSMC used to control the DC voltage of a five-level inverter is shown in Fig. 5.

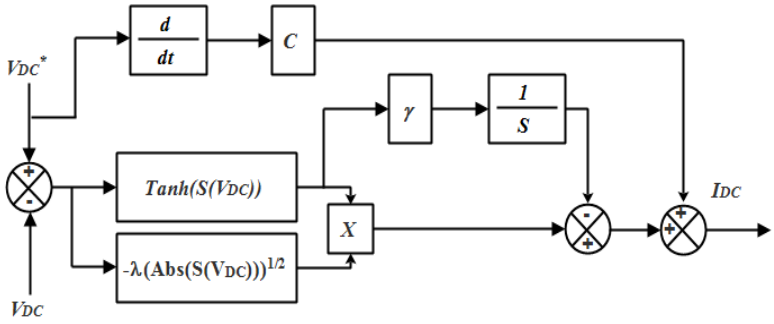


Fig. 5. Schematic diagram of DC control for the STSMC.

### 3.2.2. Clamping bridge control

Fig. 6 shows the structure of Clamping Bridge Control (CBC). It consists of a transistor ($T_i$) and a resistance ($R_p$) in series, placed parallel to the terminals of each capacity of the DC bus.

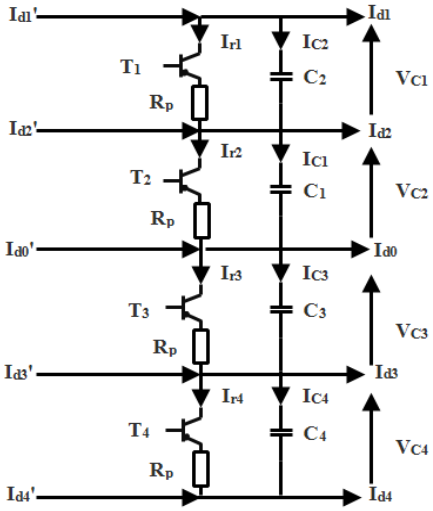


Fig.. 6. Structure of the Clamping Bridge Control circuit.

Each transistor is controlled in such a way as to ensure the stability of the input voltages of the inverter to a fixed reference value. The mathematical model of the DC bus with the CBC is defined as follows.

$$\begin{cases} C_1 \dfrac{dV_{C1}}{dt} = I_{d1}^{'} - I_{r1} - I_{d1} \\ C_2 \dfrac{dV_{C2}}{dt} = I_{d1}^{'} + I_{d2}^{'} - I_{r2} - I_{d1} - I_{d2} \\ C_3 \dfrac{dV_{C3}}{dt} = -I_{d3}^{'} - I_{d4}^{'} - I_{r3} + I_{d3} + I_{d4} \\ C_4 \dfrac{dV_{C4}}{dt} = -I_{d4}^{'} - I_{r4} + I_{d4} \\ I_{ri} = \dfrac{V_{Ci}}{R_P}; i = [1\,4] \end{cases} \tag{10}$$

Where: $I_d'$ denotes the current of the rectifier, $I_r$ is the current of CBC and $I_d$ is the current of the inverter.

The algorithm which controls the clamping bridge compares the differences ($\Delta V_{12}$) and ($\Delta V_{34}$) in the continuous voltages of each stage to zero values in real time. If the difference is not zero, the excess energy will be dissipated through the resistance. The control algorithm of the CBC is given as follows:

$$\begin{cases} \Delta V_{12} \rangle 0 \Rightarrow I_{r1} = 0 \,\&\, I_{r2} \neq 0 (T_1 = 0 \,\&\, T_1 = 1) \\ \Delta V_{12} \langle 0 \Rightarrow I_{r1} \neq 0 \,\&\, I_{r2} = 0 (T_1 = 1 \,\&\, T_1 = 0) \\ \Delta V_{34} \rangle 0 \Rightarrow I_{r3} = 0 \,\&\, I_{r4} \neq 0 (T_3 = 0 \,\&\, T_4 = 1) \\ \Delta V_{34} \langle 0 \Rightarrow I_{r3} \neq 0 \,\&\, I_{r4} = 0 (T_3 = 1 \,\&\, T_4 = 0) \end{cases} \tag{11}$$

With:

$$\Delta V_{12} = V_{C1} - V_{C2} \,\&\, \Delta V_{34} = V_{C3} - V_{C4}$$

## 4. Control and Monitoring System for the HRES

Fig. 7 shows a flowchart of the Control and Monitoring System (CMS) for the HRES connected to the power grid. The CMS receives the information on the power required by the load and the powers generated by the energy sources produced by the HRES as well as the information on THD of the currents. According to the energy quality of the HRES, four possible situations can be envisaged:

**Case 1:** $THD_{I(WE)} \leq 5.5\% \,\&\, THD_{I(PVE)} \leq 5.5\%$

First, the CMS compares the load power with the powers generated by the SERH based on this equation:

$$P_e = P_{WE} + P_{PVE} - P_{Load} \tag{12}$$

If ($Pe>0$) : The WE and PVE ensure the production of energy necessary for the load and the difference in power will be recovered by the electrical grid to be transferred to other places of the load.

$$P_{WE} + P_{PVE} = P_{Load} + P_{Grid} \tag{13}$$

If ($Pe<0$) : The power grid must react quickly to provide the difference between the power demanded by the load and that available from HRES to ensure stability between the power demand and the power generated according to this equation:

$$P_{Load} = P_{Grid} + P_{WE} + P_{PVE} \tag{14}$$

**Case 2**: $THD_{I(WE)} \leq 5.5\% \,\&\, THD_{I(PVE)} \rangle 5.5\%$

In this situation, the CMS intervenes to open the PVECS switch and the power transferred from PVE to the load or the electrical grid is zero.

$$\begin{cases} if\ (P_e \rangle 0) : P_{Load} = P_{WE} \\ if\ (P_e \langle 0) : P_{Load} = P_{Grid} + P_{WE} \end{cases} \tag{15}$$

**Case 3:** $THD_{I(WE)} \rangle 5.5\% \,\&\, THD_{I(PVE)} \leq 5.5\%$

In this situation, the CMS intervenes to open the WECS switch and the power transferred from WE to the load or the electrical grid is zero.

$$\begin{cases} if\ (P_e \rangle 0) : P_{Load} = P_{PVE} \\ if\ (P_e \langle 0) : P_{Load} = P_{Grid} + P_{PVE} \end{cases} \tag{16}$$

**Case 4**: $THD_{I(WE)} \rangle 5.5\% \,\&\, THD_{I(PVE)} \rangle 5.5\%$

In this situation, the CMS intervenes to open the WECS and PVECS switches and the powers transferred from WE and PVE to the load or the electrical grid are zeros. The electricity grid that must ensure the generation of energy to the load.

$$P_{Load} = P_{Grid} \tag{17}$$

Where: $P_e$ is the electrical power, $P_{Grid}$ is the grid power, $P_{WE}$ is the wind power, $P_{PVE}$ is the photovoltaic power and $P_{Load}$ is the load power.

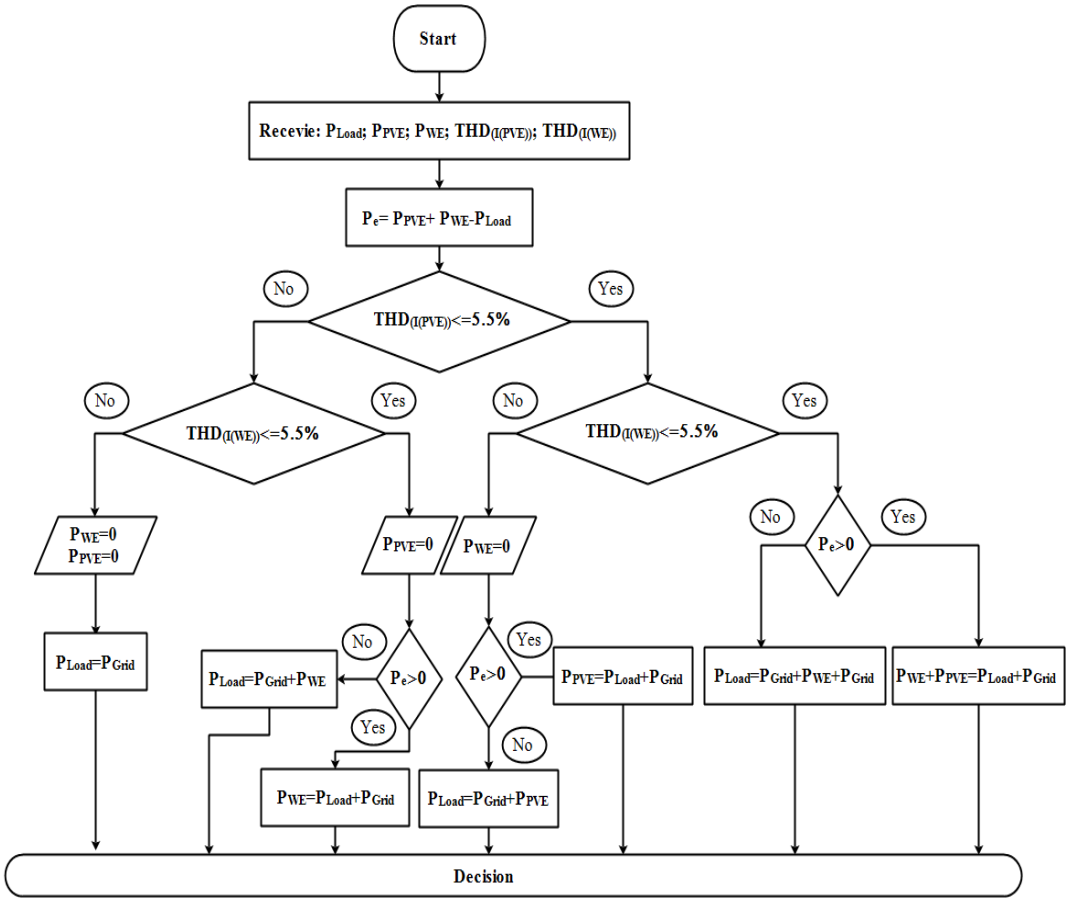


Fig. 7. Flowchart of the CMS for the HRES connected to the grid.

## 5. Simulation results and discussion

MATLAB with SimPowerSystems toolbox are used to implement the model of the proposed system of Fig. 1 and test the performance of proposed controls and supervisory system. The global model and the control scheme were simulated for two different scenarios described in the following subsections.

In order to run the simulation for the HRES connected to the power grid, meteorological data (wind speed, insolation, and temperature) are required.

The real weather data for the day 25-05-2019 was collected from the official weather website of the city of Tiaret in Algeria. Wind speed, solar irradiance, and temperature are illustrated in Figs. 8 (a), (b), and (c) respectively.

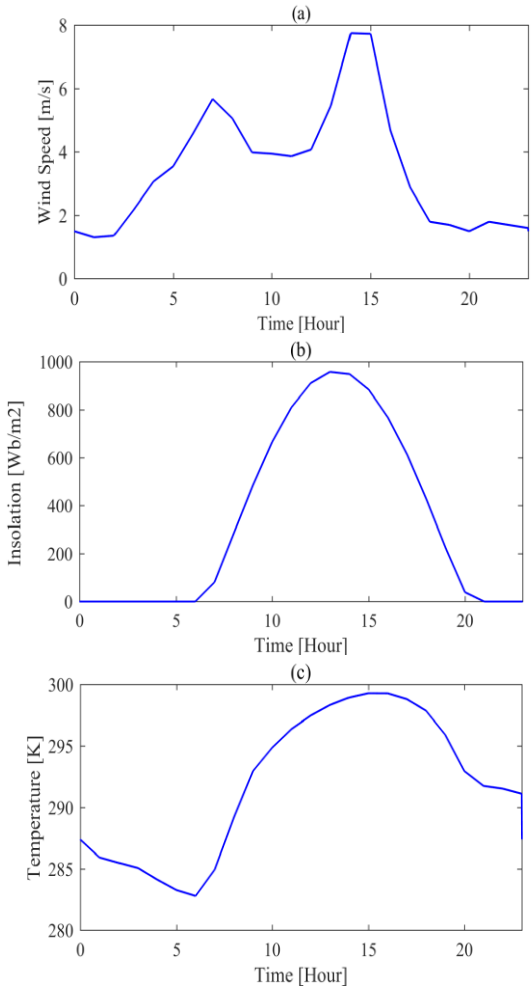


Fig. 8. Meteorological data: (a) wind speed. (b) Insolation. (c) Temperature.

The load profile used in the simulation is shown in Fig. 9. This load was estimated from average electricity consumption in a house for one day for each hour.

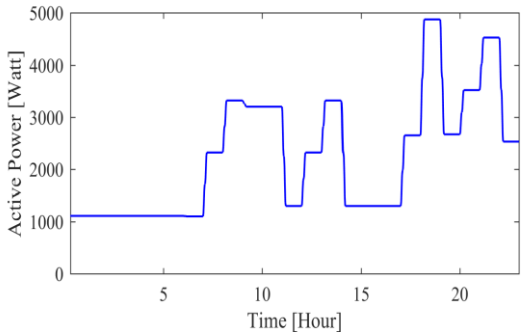


Fig. 9. Load power.

### *A. HRES connected to the grid without fault*

Fig. 10 shows the distribution of the active powers produced by the power grid, WE and PVE. First, it can be noted that the waveform of power generated by the PV system in the same as that of insolation (Fig.8.b). This indicates that the PV system is highly dependent on sunstroke. Also, the wind system generates at any instant in time its optimal power according to the speed of the available wind.

According to the flowchart of the CMS, when the power generated by the HRES is greater than that required by the load, in this case, the excess power will be transmitted to the grid to be consumed by other loads

Figs. 11 (a), (b), (c) and (d) show the waveforms of the load, power grid, WE and PVE currents respectively. From these figures, it can be seen that the waveforms of the currents are sinusoidal, stable and that their frequencies are maintained at 50 Hz.

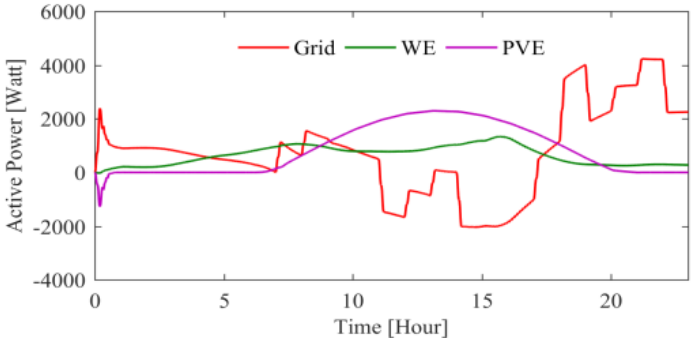


Fig. 10. Distribution of active powers generated.

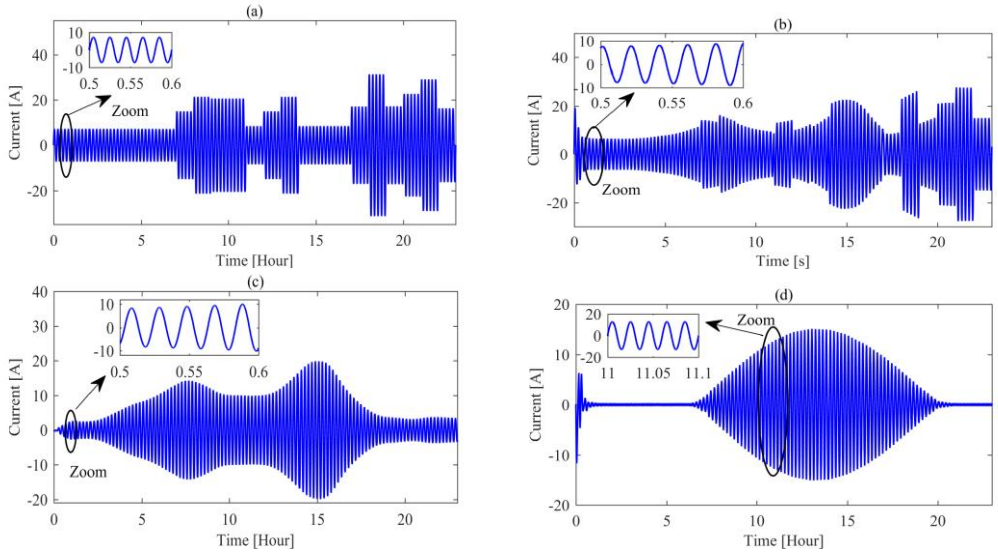


Fig. 11. The waveform of currents: (a) Load, (b) grid, (c) WE and (d) PVE.

Figs. 12 (a), (b) and (c) respectively show the analysis of the THD of the currents of WE, PVE and the grid. The THD obtained for the two RES currents have valued less than 5%. which clearly demonstrate the improved power quality. As long as this condition is verified, following the CMS flowchart both RES can be integrated into the power grid.

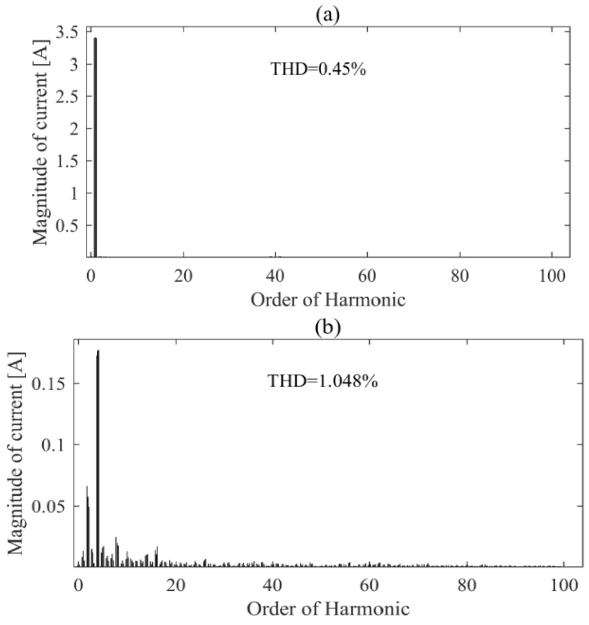

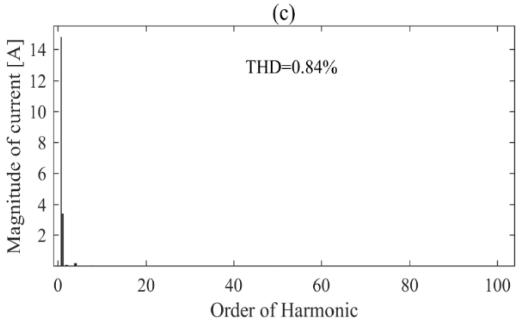


Fig. 12. THD currents for: (a) WE, (b) PVE and (c) grid.

Fig. 13 shows the shape of the DC voltage. It is clearly seen that the measured DC voltage follows its reference successfully with better performance. The DC voltage remains stable throughout this simulation. This stability is provided by the structure and control used for the five-level converters.

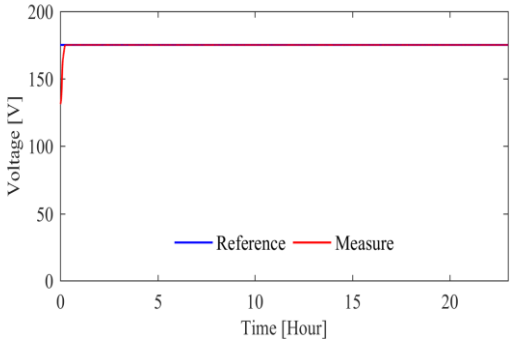


Fig. 13. DC voltage.

Fig. 14 shows the waveform of the voltage of the five-level converter. It can be noted that this voltage has the same sinusoidal waveform and has five voltage levels as expected for a five-level converter output voltage.

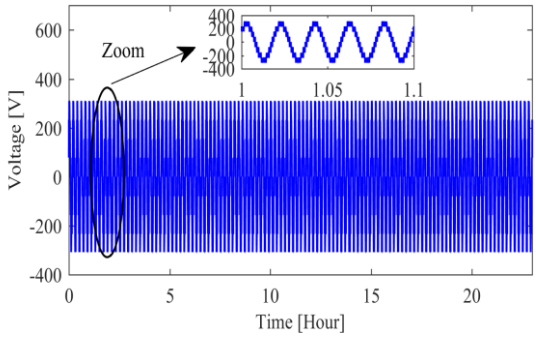


Fig. 14. Voltage of the five-level converter.

### *B. HRES connected to the grid with short circuit of three-phase*

The purpose of this scenario is to illustrate the dynamic behavior of an HRES connected to the power grid, and its impact on electrical stability during a Three-Phase Short-Circuit (TPSC) fault.

We considered the same scenario 1 but with the application of a TPSC fault in the Common Coupling Point (CCP) at *t=11 Hour* for a duration of *2min*.

Fig. 15 (a) and (b) show the distribution of the active powers and those of WE and PVE respectively.

It can be noted that the active power generated by the electrical grid has gone through three different regimes namely:

Regime 1: the system is simulated before the occurrence of a fault during the interval *t=[0 11] Hou*r, it is clear that the electrical grid, the WE and the PVE fully ensure the supply of power to the load (Fig 9) to ensure stability between the required power and the power generated.

Regime 2: between *t=[11 11.02] Hour*, during the fault of TPSC. In this case, the electricity grid becomes unstable.

Regime 3: between *t=[11.02 23] Hour*, after the cancellation of the TPSC, the HRES connected to the electrical grid intervenes quickly to restore the balance of the power flow.

These results show the efficiency and good performance of the HRES during the occurrence of TPSC fault. Because the two RES produce their optimal powers throughout the duration of stimulation without being affected by the fault.

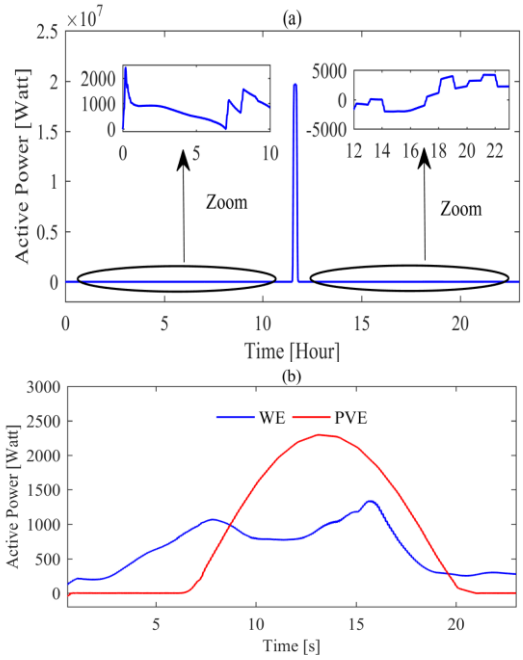


Fig. 15. Distribution of active powers generated: (a) Grid, (b) HRES

Fig. 16 shows the response of the DC voltage in this TPSC fault condition of this circuit. It is clear that the DC voltage remains stable.

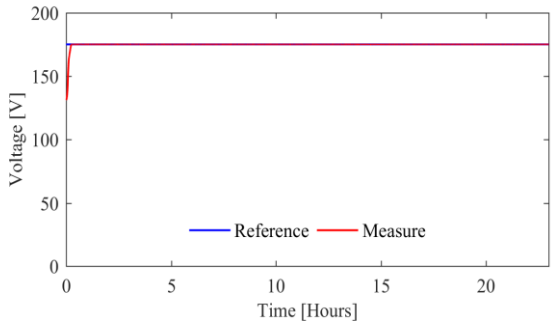


Fig. 16. DC voltage.

## 6. Conclusion

This article focused on the design and Energy Management (EM) of an HRES connected to the power grid. The design of an HRES through the use of five-level NPC converters for the purpose of improving the energy quality produced by the two RESs and the use of an advanced STSMC type controller to provide stability to the DC bus voltage. Also, a CMS has been proposed for the purpose of ensuring at any moment the energy balance between the load and the sources of production (grid, HRES) of electrical energy according to meteorological data. The proposed HRES was evaluated with two scenarios. The simulation results show the efficiency of HRES proposed by the good quality of energy produced by the two RESs and by the continuity of production of their optimal powers according to available meteorological data, load variation and for the TPSC fault.

## R E F E R E N C E S

[1] H. Al-Hamidi and J. Al Asfar, ‘Hybrid renewable energy system with minimum noise wind turbine’, Renew. Energy, vol. 114, no. Part B, pp. 581–587, Dec. 2017.

[2] B. Madaci, R. Chenni, E. Kurt, and K. E. Hemsas, ‘Design and control of a stand-alone hybrid power system’, Int. J. Hydrog. Energy, vol. 41, no. 29, pp. 12485–12496, Aug. 2016.

[3] B. Abu-Hijleh, ‘Use of Hybrid PV and Wind Turbine – Grid Connected System in a Local Emirati Home in Dubai-UAE’, Energy Procedia, vol. 100, no. Supplement C, pp. 463–468, Nov. 2016.

[4] E. Dursun and O. Kilic, ‘Comparative evaluation of different power management strategies of a stand-alone PV/Wind/PEMFC hybrid power system’, Int. J. Electr. Power Energy Syst., vol. 34, no. 1, pp. 81–89, Jan. 2012.

[5] C.-M. Hong and C.-H. Chen, ‘Intelligent control of a grid-connected wind-photovoltaic hybrid power systems’, Int. J. Electr. Power Energy Syst., vol. 55, no. Supplement C, pp. 554–561, Feb. 2014.

[6] B. Belabbas, T. Allaoui, M. Tadjine, and M. Denai, 'Power Quality Enhancement in Hybrid Photovoltaic-Battery System based on three–Level Inverter associated with DC bus Voltage Control', J. Power Technol., vol. 97, no. 4, pp. 272–282, 2017.
[7] M. M. R. Singaravel and S. A. Daniel, 'Sizing of hybrid PMSG-PV system for battery charging of electric vehicles', Front. Energy, vol. 9, no. 1, pp. 68–74, Mar. 2015.
[8] A. Tamaarat and A. Benakcha, 'Performance of PI controller for control of active and reactive power in DFIG operating in a grid-connected variable speed wind energy conversion system', Front. Energy, vol. 8, no. 3, pp. 371–378, 2014.
[9] M. Loucif, A. Boumediene, and A. Mechernene, 'Nonlinear Sliding Mode Power Control of DFIG under Wind Speed Variation and Grid Connexion', Electroteh. Electron. Autom., vol. 63, no. 3, p. 23, 2015.
[10] S. Qiang and F. Bing-Kui, 'Vector Control of Permanent Magnet Synchronous Motor Based on Sliding Mode Variable Structure Control', Univ. Politeh. Buchar. Sci. Bull. Ser. C-Electr. Eng. Comput. Sci., vol. 79, no. 3, pp. 113–122, 2017.
[11] B. Belabbas, T. Allaoui, M. Tadjine, and M. Denai, 'High Order Sliding Mode Controller Simulation by a Wind Turbine for DFIG Protection against Overcurrent.', Electroteh. Electron. Autom., vol. 65, no. 4, 2017.
[12] D. Kairous and B. Belmadani, 'Robust Fuzzy-Second Order Sliding Mode based Direct Power Control for Voltage Source Converter', Int. J. Adv. Comput. Sci. Appl., vol. 1, no. 6, pp. 167–175.
[13] B. Belabbas, T. Allaoui, M. Tadjine, and A. Safa, 'Hybrid fuzzy sliding mode control of a dfig integrated into the network', Int. J. Power Electron. Drive Syst. IJPEDS, vol. 3, no. 4, pp. 351–364, 2013.
[14] M. Mohammadi and M. Nafar, 'Fuzzy sliding-mode based control (FSMC) approach of hybrid micro-grid in power distribution systems', Int. J. Electr. Power Energy Syst., vol. 51, pp. 232–242, 2013.
[15] A. Swikir and V. Utkin, 'Chattering analysis of conventional and super twisting sliding mode control algorithm', in Variable Structure Systems (VSS), 2016 14th International Workshop on, 2016, pp. 98–102.
[16] B. Belabbas, T. Allaoui, M. Tadjine, and M. Denai, 'Comparative study of back-stepping controller and super twisting sliding mode controller for indirect power control of wind generator', Int. J. Syst. Assur. Eng. Manag., pp. 1–12.
[17] D. Yang, M. Kang, J. Kim, J. Hong, and Y. C. Kang, 'Stable stepwise short-term frequency support of a DFIG-based wind farm', Int. Trans. Electr. Energy Syst., vol. 28, no. 3, p. e2495, 2018.
[18] M. Ionescu, 'P&O Maximum Power Point Regulation Model for Two Stage Grid Connected PV Systems', Univ. Politeh. Buchar. Sci. Bull. Ser. C-Electr. Eng. Comput. Sci., vol. 80, no. 2, pp. 85–96, 2018.
[19] H. Wu, S. Wang, B. Zhao, and C. Zhu, 'Energy management and control strategy of a grid-connected PV/battery system', Int. Trans. Electr. Energy Syst., vol. 25, no. 8, pp. 1590–1602, 2015.
[20] Q. Zhang, Y. Liu, and C. Wang, 'The elimination of leakage currents in the neutral point clamped photovoltaic grid-connected inverter by the improved space vector pulse width modulation method', Int. J. Sustain. Energy, no. ahead-of-print, pp. 1–13, 2013.
[21] A. Fri, R. E. Bachtiri, and A. E. Ghzizal, 'A Comparative Study of Three Topologies of Three-phase (5L) Inverter for a PV System', Energy Procedia, vol. 42, pp. 436–445, 2013.